The physical balances in subseafloor hydrothermal convection cells

Tim E. Jupp[1]

BP Institute for Multiphase Flow, University of Cambridge, Cambridge, U.K.

Adam Schultz[2]

School of Earth, Ocean and Planetary Sciences, Cardiff University, Cardiff, U.K.

Abstract. We use a simplified model of convection in a porous medium to investigate the balances of mass and energy within a subseafloor hydrothermal convection cell. These balances control the steady-state structure of the system, and allow scalings for the height, permeability and residence time of the 'reaction zone' at the base of the cell to be calculated. The scalings are presented as functions of (1) the temperature T_D of the heat source driving the convection and (2) the total power output Φ_U. The model is then used to illustrate how the nonlinear thermodynamic properties of water may impose the observed upper limit of $\sim 400°$C on vent temperatures. The properties of water at hydrothermal conditions are contrasted with those of a hypothetical 'Boussinesq fluid' for which temperature variations in fluid properties are either linearised or ignored. At hydrothermal pressures, water transports a maximum amount of energy by buoyancy-driven advection at $\sim 400°$C. This maximum is a consequence of the nonlinear thermodynamic properties of water, and does not arise for a simple 'Boussinesq fluid'. Inspired by the 'Malkus hypothesis', and by recent work on dissipative systems, we speculate that convection cells in porous media attain a steady state in which the upwelling temperature T_U maximises the total power output of the cell. If true, this principle would explain our observation (in previous numerical simulations) that water in hydrothermal convection cells upwells at $T_U \sim 400°$C when driven by a heat source above $\sim 500°$C.

1. Introduction

At mid–ocean ridge spreading centres, magmatic heat sources drive the convection of seawater through the oceanic crust. Water heated by this process is then returned to the oceans at sites of hydrothermal venting, where no hydrothermal vent hotter than 405°C has ever been observed. The aims of this paper are (1) to quantify the fundamental physical balances in a 2-d model of hydrothermal convection and (2) to investigate in detail how the thermodynamic properties of water might limit hydrothermal vent temperatures to $\sim 400°$C. At hydrothermal pressures, the density and viscosity of water are highly nonlinear functions of temperature near $\sim 400°$C, and it has been suggested for some years that this behaviour might be responsible for the upper limit on vent temperatures [e.g. Bischoff and Rosenbauer, 1985; Johnson and Norton, 1991]. It is known that the thermodynamic properties of water affect the onset of convection and the overall rate of heat transfer in convection cells operating across a small temperature difference (say $\Delta T = 10°$C) [Straus and Schubert, 1977; Dunn and Hardee, 1981; Ingebritsen and Hayba, 1994]. If ΔT is sufficiently small, the variation of fluid properties with temperature can be linearised or ignored (the 'Boussinesq Approximation' [Phillips, 1991]) and it can be shown that cells operating near the critical point of water (~ 22 MPa, $\sim 374°$C) transfer heat much more rapidly than cells driven by the same ΔT at other points in $p - T$ space. Such 'superconvection' suggests that hydrothermal systems might be very effective at heat transfer, but it is insufficient to explain the apparent limit to vent temperatures. Real systems operate over a large temperature difference (suggeting that the Boussinesq Approxmation is inappropriate) and they seem to be limited to a maximum vent temperature of $\sim 400°$C. To explain this, the focus of investigation must move from the overall heat transfer to the internal temperature structure of the cell.

In a previous paper we presented numerical simulations of hydrothermal convection and showed that the nonlinear thermodynamic properties of water constrain the temperature of upwelling flow in hydrothermal systems to be $\sim 400°$C when driven by a heat source at sufficiently high temperature [Jupp and Schultz, 2000]. In the present paper, we explore the physics behind our previous numerical observations. The crucial feature of the nonlinear properties of water at seafloor pressures is that a maximum amount of heat energy is transported in buoyancy-driven flow if the water is at $\sim 400°$C . This behaviour is in stark contrast to that of a hypothetical 'Boussinesq fluid' for which there is no such maximum (Figure 4f).

[1]Now at Centre for Ecology and Hydrology, Natural Environment Research Council, Huntingdon, U.K.

[2]Now at College of Oceanic and Atmospheric Sciences, Oregon State University, Corvallis, Oregon, U.S.A.

Paper number .
0148-0227/04/$9.00

In this paper we investigate hydrothermal convection by considering the balances of mass and energy in a single convection cell in a homogeneous 2-d porous medium. In general, it is possible for multiple convection cells to arise above a single heat source if the imposed heating is sufficiently strong. In our numerical simulations, however, we observed only single convection cells for plausible parameter values [Jupp and Schultz, 2000]. For this reason we shall assume a flow structure with a single upwelling plume. In all other respects the flow geometry is not specified *a priori* but emerges as a solution of the governing equations. Our simplified model of convection therefore lies somewhere in between a full '2–d' model in which flow is unconstrained and a 'pipe' model in which flow is constrained to lie within a pre-existing U-shaped geometry [Lowell and Germanovich, 2004].

2. The expected structure of a subseafloor convection cell

A schematic picture showing the expected structure of a subseafloor convection cell is shown in Figure 1. The energy required to drive the convection of hydrothermal fluids is supplied by the top surface of a magmatic source body. This is typically a magma chamber, but could equally be a dike or sill [Cann and Strens, 1982; Richardson *et al.*, 1987]. The temperature T_M of the magma body is governed by the melting point of magma and is usually taken to be $T_M \sim 1200°\mathrm{C}$ [Morton and Sleep, 1985; Lowell *et al.*, 1995]. In a typical situation, a magma chamber is located at a depth $H \sim 1000$ m below the seafloor and has a width $2L \sim 1000$ m [Detrick *et al.*, 1987].

The rock immediately above the magma chamber is thought to be impermeable to seawater. This is because rock at sufficiently high temperatures flows in a ductile fashion when subjected to strain and so cannot provide permeable pathways by cracking. For this reason, the seafloor is usually treated as impermeable at temperatures above some 'brittle-ductile transition temperature' T_D [Lister, 1974]. It follows that heat from the solidifying magma chamber is transferred conductively through an impermeable layer of thickness H_I to the overlying permeable seafloor.

Within the permeable layer, fluid motion is driven by heat supplied at temperature T_D and so we may also interpret T_D as a 'driving temperature' for convective flow with the general flow pattern indicated in Figure 1. Cold seawater ($\sim 2°\mathrm{C}$) downwells through a broad 'recharge zone' where temperatures are relatively low ($\ll 350°\mathrm{C}$) [Alt, 1995]. As the water percolates down through the subseafloor, the temperature begins to rise and the fluid interacts chemically with the surrounding rock, leading to an exchange of chemical elements between the evolved seawater and the crust. After the recharge zone, which is characterised by descending fluid flow, the fluid enters a region known as the reaction zone which is thought to occur at the maximum penetration depth of the fluid and is characterised by temperatures in excess of 375°C [Berndt *et al.* 1989]. Estimates of the typical residence time of fluids in the reaction zone can be made from radioisotope studies and range from less than 3 years [Kadko and Moore, 1988] to 20 years [Grasty *et al.*, 1988]. Later in this paper, we shall compare these estimated residence times with predictions based on the physical balances in a simple model of two dimensional convection. Fluid leaves the reaction zone at an 'upwelling temperature' T_U and so the reaction zone spans a temperature range from T_U at its top to T_D at its base. The subsequent vertical temperature gradient drives a conductive heat flux within the base of the permeable layer. We stress that this constitutes the second of two distinct 'conductive layers' in this model: (1) the impermeable layer of thickness H_I in which there is no fluid flow at all and (2) the reaction zone of thickness H_R in which a vertical conductive heat flux supplies energy to a predominantly horizontal flow of water. Thermal calculations suggest that both of these conductive layers must be relatively thin ($H_C \sim H_R \sim 100$ m) in order to maintain the typical power output ($\sim 100 - 1000$ MW) of a hydrothermal system [Lowell and Germanovich, 1994, 2004; Schultz *et al.*, 1992].

After the reaction zone, the convecting water enters a discharge zone through which it ascends to hydrothermal venting sites on the seafloor (Figure 1). The typical lateral dimensions of a hydrothermally active region of the seafloor (< 100 m) are considerably less than the expected lateral dimension of the magma chamber ($2L \sim 1000$ m) and so the discharge zone is often said to be 'focussed'. It is possible that high permeability pathways, due to fractures, faults or textural inhomogeneities in the crust, might serve to focus the flow in the discharge zone. It must be stressed, however, that these inhomogeneities in crustal permeability are not strictly necessary in order to impose the required structure on the cell. Some degree of focussing of the upwelling fluid is inevitable in any convection cell, even in the absence of any high permeability pathways [Phillips, 1991; Dickson *et al.*, 1995].

After ascending through the discharge zone, the convecting fluid is expelled from hydrothermal vents on the seafloor

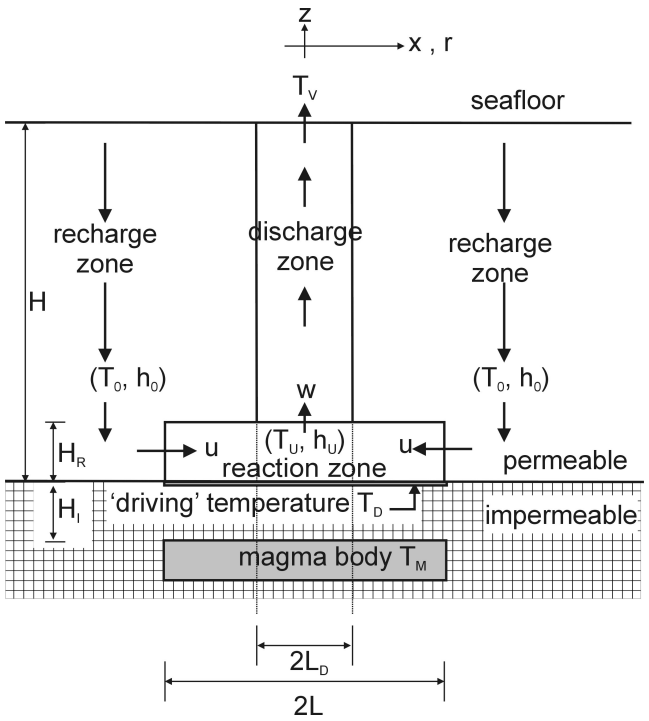

Figure 1. Cross–section showing the expected structure of a subseafloor hydrothermal convection cell and the schematic model of convection which is explored here. A list of symbols is given at the end of the paper.

at a vent temperature T_V which is typically between 350°C and 400°C in the case of black smoker venting. The cooling of the ascending fluid in the discharge zone ensures that $T_V \leq T_U$.

There are several mechanisms which might cause the fluid to cool as it rises through the discharge zone. These include conductive heat loss, adiabatic cooling and the entrainment of cooler fluids [Lowell *et al.*, 2003] . (A fourth mechanism - heating or cooling due to chemical reactions - probably operates in hydrothermal systems, but the attendant changes in temperature are likely to be insignificant on the scales considered here. For example, Lowell and Rona (2002) calculate that temperature changes due to the serpentinization of peridotite are probably at most a few tens of Kelvin for a typical ridge–axis system.) Conductive heat loss in the ascending fluid is caused by horizontal temperature gradients in the discharge zone while adiabatic cooling is a consequence of depressurisation. For example, if the hydrothermal vent field lies 2.5 km below sea level and lies 1 km above the reaction zone, then the upwelling fluid depressurises from $\sim$ 35 MPa to $\sim$ 25 MPa during its ascent through the discharge zone. Under adiabatic cooling alone, water leaving the reaction zone at $\sim$ 400°C would cool by $\sim$ 10°C on ascent to the seafloor [Haar *et al.*, 1984]. The presence of other mechanisms for heat loss means that the true degree of cooling in the discharge zone is somewhat greater. In any case, the upwelling temperature T_U provides an upper bound for the vent temperature T_V.

2.1. Observational constraints

The most rigid constraint on cell structure is provided by the temperature T_V of the fluid expelled at seafloor vents. No hydrothermal effluent hotter than 405°C has ever been observed [Von Damm *et al.*, 2003]. This is remarkable because it is so much less than the temperature ($T_M \sim 1200$°C) of the magmatic heat source [Lister, 1995; Lowell *et al.*, 1995; Wilcock, 1998]. Consequently, a successful model for hydrothermal circulation must explain the discrepancy of up to 800°C between the inferred temperature of the heat source and the observed temperature of the effluent at the seafloor.

Palaeo–oceanic crust exposed on land in ophiolite complexes provides further evidence to support the expected structure described above. In locations such as Cyprus and Oman, fossil hydrothermal systems are exposed in cross–section. It is therefore possible to infer the temperature structure that existed at depth within the fossil system using fluid inclusion geothermometry [Cowan and Cann, 1988] and by analysing the hydrothermal metamorphic mineral assemblages present. For example, Gillis and Roberts (1999) report measurements made at a section of the Troodos Ophiolite in Cyprus. They interpret this section to represent a layer of conductive heat transport in which there was a linear temperature drop from $\sim$ 1000°C to $\sim$ 400°C over a vertical distance of $\sim$ 100 m. Thus, this region can be likened to the conductive zones of thickness H_R and H_I in the prototype hydrothermal system of Figure 1. Furthermore, their data are consistent with the typical thickness $H_R \sim H_I \sim 100$ m inferred from thermal balance calculations [Lowell and Germanovich, 1994, 2004].

Measurements of the temperature and chemical composition of hydrothermal effluent can be made at active seafloor hydrothermal systems. Although these data are collected on the seafloor, they can be used to constrain the conditions within the convection cell at depth below the seafloor. An example of this process is the application of geothermometry and geobarometry [e.g. Bischoff and Rosenbauer, 1985; Von Damm and Bischoff; 1987]. The data consist of the measured temperature of the vent T_V and the measured concentration of a dissolved chemical species (such as silica) in the vent fluid. If it is assumed that the silica has been leached from basalt and that the fluid has undergone negligible conductive heat loss (and negligible chemical reaction) on its ascent to the seafloor, then the pressure and temperature of the reaction zone from which it ascended can be estimated. Studies using these techniques reach a fairly consistent conclusion - that the reaction zone is typically $\sim$ 1 km below the seafloor and a few tens of degrees hotter than the 350°C - 400°C which is typical of the hydrothermal vents themselves [Von Damm *et al.*, 1985; Campbell *et al.*, 1988].

In terms of our model, we emphasise that these techniques use the state of the fluid at the vent to infer the $p-T$ conditions at which the fluid was most recently in physical and chemical equilibrium with the subseafloor. Thus, it is only the conditions at the boundary of the reaction zone and the discharge zone which can be estimated. It is important to note that a typical geothermometry estimate of $T_U \sim 400$°C does not preclude the possibility that the fluid reached much higher temperatures at some earlier point in its history. It should also be noted that the reaction zone depths inferred by geobarometry ($\sim$ 1 km) are broadly similar to the magma chamber depths inferred by seismic imaging of the seafloor [e.g. Detrick *et al.*, 1987; Toomey *et al.*, 1994; Dunn et al., 2000].

2.2. Summary of cell structure

In summary, a successful model of a typical hydrothermal convection cell should display the following features:

(i) A magmatic heat source of width $2L \sim 1000$ m and temperature $T_M \sim 1200$°C lying at a depth $H \sim 1000$ m below the seafloor. Heat from this magma chamber drives convection of seawater in the oceanic crust.

(ii) A seafloor pressure in the range 20 MPa - 50 MPa, corresponding to a depth below sea level of 2 km - 5 km.

(iii) A relatively thin ($H_I \sim 100$ m) impermeable layer between the magmatic heat source (at temperature T_M) and the base of the permeable seafloor at (temperature T_D).

(iv) A similarly thin ($H_R \sim 100$ m) thermal boundary layer within the permeable seafloor characterised by temperatures in excess of 400°C and predominantly horizontal fluid flow.

(v) Convection in the permeable seafloor driven by heat supplied at the 'driving temperature' T_D. It has been suggested that the ductile transition occurs at $T_D \approx 500-700$°C in hydrothermal systems [Lister, 1974]. On the other hand, rock at higher temperatures may have a permeability structure that is not provided by cracking and so it is hard to exclude the possibility that water may penetrate into subseafloor systems at significantly higher temperatures. Because of this uncertainty we do not impose any particular value on the driving temperature T_D in this analysis - except for the obvious limits $T_U \leq T_D \leq T_M$. We show below that our results are essentially insensitive to T_D provided that $T_D \geq 500$°C.

(vi) A relatively narrow plume (or discharge zone) of width $2L_D$ through which upwelling fluid at $T_U \sim 400$°C ascends to the seafloor.

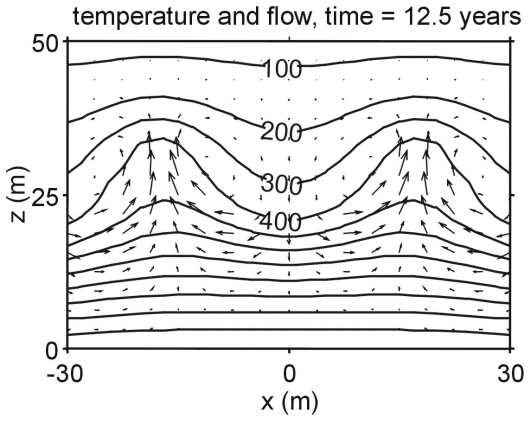

Figure 2. The evolving pattern of convection at early times in the numerical simulations. This figure shows a small region at the bottom of the permeable seafloor shown in Figure 1, at the early stages of the simulation, before a steady state has been reached. The temperature and flow fields are shown just after plume formation. Advection has just begun to distort the thermal structure. (As the simulation progresses to steady state, these two plumes coalesce to form a single plume of the type shown in Figure 3). Isotherms are drawn from 100°C (top) to 1100°C (bottom) in increments of 100°C. Vectors are of Darcy velocity. Figure adapted from Jupp and Schultz, 2000.

(vii) Hydrothermal vents on the seafloor, through which fluid emerges at temperature T_V. Observational evidence suggests that T_V for focussed, black smoker fluids typically lies between ~ 350°C and ~ 400°C.

(vii) A total power output of perhaps $100-1000$ MW per hydrothermal system.

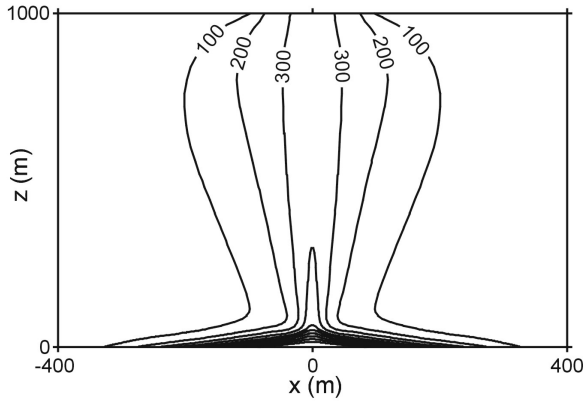

Figure 3. The steady state temperature distribution in a numerical simulation of a hydrothermal cell with driving temperature $T_D = 1200$°C. The overall temperature structure of the convection cell is shown, illustrating the distinction between the reaction zone and the discharge zone. Isotherms from 100°C to 1100°C are drawn, in increments of 100°C. Flow vectors are omitted for clarity. Flow is downwards at the sides, towards the centre at the base and upwards in the centre. Figure adapted from Jupp and Schultz, 2000.

Following Jupp and Schultz (2000) we argue here that a 2-d model of convection in a porous medium produces a structure which is consistent with all of these constraints. In particular, we argue that the nonlinear thermodynamic properties of water ensure that fluid upwells at $T_U \sim 400$°C for any sufficiently high driving temperature $T_D \geq 500$°C. For simplicity, we assume that the porosity and permeability of the seafloor are constant and homogeneous within any given region of the convection cell (such as the recharge zone, reaction zone or discharge zone). This is a considerable simplification, but it allows the influence of the thermodynamic properties of water to be considered in isolation. Thus, although the real ocean crust is highly inhomogeneous, we shall show that this inhomogeneity is not necessary to explain the principal structural features of hydrothermal convection as outlined above. The general properties of convection cells in porous media – coupled with the thermodynamic properties of water – are sufficient to explain this structure.

2.3. Results of numerical simulations

Jupp and Schultz (2000) used numerical simulations incorporating the full thermodynamic properties of water to study hydrothermal convection in a homogeneous porous medium at seafloor pressures. They studied convection driven by a heat source at temperature $T_D \leq 1200$°C in an initially cold permeable layer and observed the subsequent evolution of the system as heat was transported by conduction and convection. They observed both the time evolution of the system and its final steady state. Two key results emerged from their study: (i) the first convective instability occurs at ~ 400°C when the system is evolving and (ii) the final steady state is one in which fluid upwells at $T_U \sim 400$°C. Both of these results apply for any driving temperature T_D between 500°C and 1200°C.

The observation concerning the first instability can be interpreted in terms of the theoretical development introduced by Howard (1964). At very small times after the introduction of a heat source at temperature T_D, the evolution of the temperature field in the permeable layer is controlled entirely by conduction. Heat diffuses into the permeable layer in a thin boundary layer which grows with time. Convective motion may exist but it is insignificant in terms of the thermal balance, which is dominated overwhelmingly by conduction. Eventually the lengthscale over which heat has diffused into the permeable layer becomes sufficiently large that a convective instability develops. At this point plumes form (Figure 2). Numerical simulations and a simple physical argument show that the rate of advective accumulation of thermal energy in the evolving thermal boundary layer is greatest at ~ 400°C for water at hydrothermal pressures [Jupp and Schultz, 2000]. It follows that the growth rate of the instability is greatest at ~ 400°C. It is suggested that this controls the temperature at which plumes form.

The observation concerning the steady state attained by the system will be considered in detail in this present paper. In the steady state the upwelling temperature in the simulations (Figure 3) was found to be $T_U \sim 400$°C for any driving temperature T_D in the range ~ 500°C to ~ 1200°C.

3. A simplified model for hydrothermal convection

We now consider how a simplified model in two dimensions can be used to elucidate the physics controlling the

structure observed in the numerical simulations. We consider the balances of mass and energy in a geometrically simplified reaction zone in order to derive scalings for the system. The scaling arguments used here are based on those of Phillips (1991), but with two important differences. Firstly, we retain the full, nonlinear thermodynamic properties of water wherever possible so that their influence on cell structure can be considered. Secondly, we introduce an extra variable into the analysis - the temperature T_U of the upwelling fluid at the base of the discharge zone.

For the moment, we consider a two–dimensional convection cell in Cartesian geometry in which the heat source is taken to extend infinitely along the ridge axis (or 'into the page' in terms of the sketch in Figure 1). In section 6, we shall consider the case of radial geometry where the heat source is taken to be circular in plan form. We suppose that on a macroscopic scale, the fluid flow can be considered as flow through a porous medium and so is governed by Darcy's Law. There is little horizontal flow above the reaction zone and therefore horizontal pressure gradients must be negligible. Below this level, however, there is considerable horizontal flow from the recharge zone into the reaction zone. We suppose for simplicity that the physical properties of the water at the upwelling temperature T_U (when it leaves the reaction zone) are representative of the conditions within the reaction zone as a whole. Thus, within the reaction zone there is movement of hot fluid of approximate density ρ_U and approximate viscosity μ_U (here and subsequently, the subscript 'U' denotes the value of a fluid property at the upwelling temperature T_U). The flow in the reaction zone is predominantly horizontal, and so the vertical pressure gradient within the reaction zone must be approximately equal to the hot hydrostatic value $g\rho_U$. Outside the reaction zone, at the base of the cell, the flow of cold water (of density ρ_0) is also predominantly horizontal. In this region, therefore, the vertical pressure gradient must be approximately equal to the cold hydrostatic value $g\rho_0$. At the base of the cell, the difference between the hot and cold hydrostatic pressure regimes – inside and outside the reaction zone – applies over a vertical distance H_R. It follows that the horizontal pressure difference driving fluid into the reaction zone is given, in approximate terms, by

$$\Delta p \sim (\rho_0 - \rho_U)\, g H_R. \tag{1}$$

This pressure difference operates over a horizontal distance L, and so by Darcy's law the horizontal volume flux (or Darcy velocity) of fluid flowing laterally into the reaction zone has approximate magnitude

$$u \sim \frac{k_R}{\mu_U}\frac{\Delta p}{L} = g k_R \frac{(\rho_0 - \rho_U)}{\mu_U}\frac{H_R}{L}, \tag{2}$$

where k_R is the permeability of the reaction zone. Above the level of the reaction zone horizontal pressure gradients must be negligible as there is negligible horizontal flow. The vertical pressure gradient must be less than the cold hydrostatic $g\rho_0$ (so that cold water can be driven downwards) and greater than the hot hydrostatic value $g\rho_U$ (so that hot water can be driven upwards). The discharge zone in a 2–d convection cell is much narrower than the recharge zone and so presents a greater total resistance to a given volume flux of water. It follows that the vertical pressure gradient (above the level of the reaction zone) is much closer to cold hydrostatic than hot hydrostatic. The vertical volume flux of fluid in the discharge zone is therefore given, approximately, by

$$w \sim g k_D \frac{(\rho_0 - \rho_U)}{\mu_U}, \tag{3}$$

where k_D is the permeability of the discharge zone. We emphasise that the permeability of the reaction zone k_R may be different from the permeability of the discharge zone k_D. There are two reasons why these permeabilities should be considered independently. Firstly, the flow is chiefly horizontal in the reaction zone but vertical in the discharge zone. Thus, if the permeability of the seafloor were not isotropic then k_R would not necessarily be equal to k_D. Secondly, it may be that the two permeabilities evolve differently over time due to the precipitation or dissolution of minerals. The reaction zone is characterised by fluids flowing up a temperature gradient, while the discharge zone contains fluid flowing down a temperature gradient. Since the aqueous solubility of minerals depends on temperature, it follows that a mineral which is dissolved in the reaction zone might precipitate as it enters the discharge zone (and vice versa).

Returning to the structure of convection cells, we note that fluid enters the reaction zone with volume flux u and leaves with volume flux w. We neglect any changes of fluid mass due to hydration and dehydration reactions. It then follows from Figure 1 shows that the conservation of fluid mass in the reaction zone is expressed by the balance

$$2\rho_U u H_R \sim 2\rho_U w L_D. \tag{4}$$

Equations 2, 3 and 4 can then be combined to express the mass balance in the alternative form

$$k_R H_R^2 \sim k_D L_D L. \tag{5}$$

We now consider the energy balance of the reaction zone. Thermal energy enters the reaction zone by conduction from below and leaves by advection into the discharge zone at temperature T_U. The vertical temperature drop driving the conduction of heat into the reaction zone is given by the difference between the driving temperature T_D and the upwelling temperature T_U. It follows that the convective system is driven by a vertical conductive heat flux of approximate magnitude $\lambda(T_D - T_U)/H_R$ which operates over a horizontal distance $2L$ where λ is the thermal conductivity. The advective heat transport consists of a vertical volume flux w operating over a horizontal distance $2L_D$. The ascending fluid has been heated in the reaction zone so that its specific enthalpy has been raised from a 'cold' value h_0 at temperature T_0 to a 'hot' value h_U at the upwelling temperature T_U. Neglecting the enthalpy of chemical reactions, the conservation of energy in the reaction zone is then expressed by the following balance between conductive and advective heat transport:

$$2L\frac{\lambda\,(T_D - T_U)}{H_R} \sim 2\rho_U (h_U - h_0) w L_D. \tag{6}$$

This can be re–arranged (using equation 3) to give:

$$\frac{L\lambda\,(T_D - T_U)}{L_D H_R} \sim g k_D \left[\frac{\rho_U (h_U - h_0)\,(\rho_0 - \rho_U)}{\mu_U}\right]. \tag{7}$$

At this point it is helpful to define a thermodynamic variable F_U based on the quantity in square brackets above. This quantity is a function of the thermodynamic state of

the water at the upwelling temperature T_U and is a measure of its ability to transport heat by buoyancy–driven convection in a cold hydrostatic pressure gradient $g\rho_0$. We follow Lister (1995) in using the term 'fluxibility' to describe this quantity, which is defined by

$$F = \frac{\rho(h - h_0)\,(\rho_0 - \rho)}{\mu} \tag{8}$$

for fluid at arbitrary temperature T. The vertical advective heat flux at the base of the discharge zone (measured in $\mathrm{W.m^{-2}}$) is proportional to the fluxibility: gk_DF_U. This heat flux is measured relative to a 'ground state' enthalpy h_0 which corresponds to cold seawater. It follows that the heat flux gk_DF_U can be interpreted as the rate at which energy would be liberated from the flow (per unit area at the base of the discharge zone) when upwelling water with enthalpy h_U is returned to the cold 'ground state' h_0. This is precisely what happens when hydrothermal effluent enters the ocean and cools.

4. The thermodynamic properties of pure water as functions of pressure and temperature

We now consider how the fluxibility F of upwelling water varies as a function of pressure and temperature under hydrothermal conditions. In order to do so, and to elucidate the underlying physics, we consider in turn the various thermodynamic and transport properties of water on which the fluxibility depends. One of our main aims in this paper is to highlight the differences between the properties of a hypothetical 'Boussinesq fluid' (for which the temperature dependence of basic thermodynamic properties is either linearised or ignored) and the real thermodynamic behaviour of pure water at high pressure and temperature. Accordingly, we shall calculate the thermodynamic properties in two ways - (i) using the full nonlinear properties of water and (ii) using the simplifications inherent in the Boussinesq approximation. For simplicity, we restrict attention to pure water rather than the multi–component aqueous solution that flows through a real hydrothermal system. This allows us to examine the physics of convection without following the evolving chemistry of the fluid. The thermodynamic properties of pure water and brine are quantitatively similar with the single important difference that brine can boil at all pressures whereas pure water cannot boil at pressures above the critical pressure of 22 MPa. At pressures above 22 MPa, pure water undergoes a smooth transition from a 'liquid–like' state to a 'gas–like' state instead of the abrupt phase transition which constitutes boiling [Bischoff and Pitzer, 1985]. Consequently, our system is one in which the convecting fluid cannot co–exist as both a liquid and a gas at a given point in space. In all other respects, however, the thermodynamic behaviour of pure water is qualitatively equal (and quantitatively very similar) to the thermodynamic behaviour of a brine.

The temperature dependence of the density of the upwelling water is of fundamental importance as it provides the buoyancy force which drives the circulation. Figure 4*a* shows the variation in the density of pure water ρ over a range of pressures and temperatures relevant to seafloor hydrothermal systems. The density varies greatly with temperature and little with pressure, with a marked density drop occurring between $\sim 400^\circ$C and $\sim 500^\circ$C for all seafloor pressures. If the pressure is less than the critical pressure of 22 MPa (equivalent to $\sim$ 2.2 km cold hydrostatic head), this density drop is discontinuous, and is caused by a change of state from liquid to vapour as the water boils. If the pressure is greater than 22 MPa, however, pure water cannot coexist as two separate phases and does not boil. In this case the density becomes a continuous (but nonlinear) function of temperature. There is still a fairly sharp drop in density at $\sim 400^\circ$C, but it is not caused by boiling because there is no discontinuity and no phase change. For seafloor pressures above 22 MPa, water undergoes a smooth transition from a 'liquid–like' state below $\sim 400^\circ$C to a 'gas–like' state above $\sim 400^\circ$C. When water is in the liquid–like state the temperature dependence of the density is approximately linear: $\rho \approx \rho_0\,[1 - \alpha\,(T - T_0)]$. In the gas–like state, on the other hand, the density variations can be approximated by the behaviour of a perfect gas: $\rho \approx \beta p/T$ where $\beta \sim 2.3 \cdot 10^{-3}$ $\mathrm{kg.K.J^{-1}}$. This highly nonlinear behaviour can be contrasted with the behaviour of a Boussinesq fluid (shown by dashed lines in Figure 4*a*).

When a Boussinesq fluid is considered in the context of convection equations, the temperature dependence of the fluid density is ignored in all terms except the term relating to the fluid's buoyancy. Thus, the density ρ_{Bsq} of a Boussinesq fluid is given by:

$$\rho_{Bsq} = \begin{cases} \rho_0\,[1 - \alpha\,(T - T_0)] & \text{(buoyancy terms)}, \\ \rho_0 & \text{(other terms)}. \end{cases} \tag{9}$$

Figure 4*a* shows that, for seafloor hydrothermal systems, the Boussinesq approximation for fluid density is reasonable only for water below about 200°C. At the higher temperatures characteristic of the reaction and discharge zones the Boussinesq approximation is inappropriate [Wilcock, 1998].

We now consider the specific enthalpy $h - h_0$ which measures the thermal energy content of water (in $\mathrm{J.kg^{-1}}$) relative to water at the cold temperature T_0. Figure 4*b* shows the variation in specific enthalpy $h - h_0$ of water under hydrothermal conditions. The specific enthalpy of water at hydrothermal conditions is essentially independent of pressure and is (globally) an approximately linear function of temperature. This means (in contrast to the behaviour of the density) that the specific enthalpy of water in hydrothermal systems is given to a reasonable approximation by the Boussinesq value h_{Bsq}:

$$h \approx h_{Bsq} = h_0 + c_p\,(T - T_0)\,. \tag{10}$$

Although the specific enthalpy is approximately linear in temperature, equation 8 suggests that the volumetric enthalpy $\rho(h - h_0)$ is of greater physical significance to the advective transport of heat. The volumetric enthalpy is a measure of the energy content of the fluid per unit volume (Figure 4*c*). Unlike the specific enthalpy $h - h_0$, the volumetric enthalpy is affected by the great variability in density, and so it is not always an increasing function of temperature. At seafloor hydrothermal pressures, the volumetric enthalpy is maximised at $\sim 400^\circ$C. Consequently a unit volume of water at $\sim 400^\circ$C contains more thermal energy than a unit volume of water at any other temperature. This is because the expansion of water is such when heated beyond 400°C that the thermal energy per unit volume begins to decrease as the temperature is increased, even though the thermal energy per unit mass continues to increase. This nonlinear

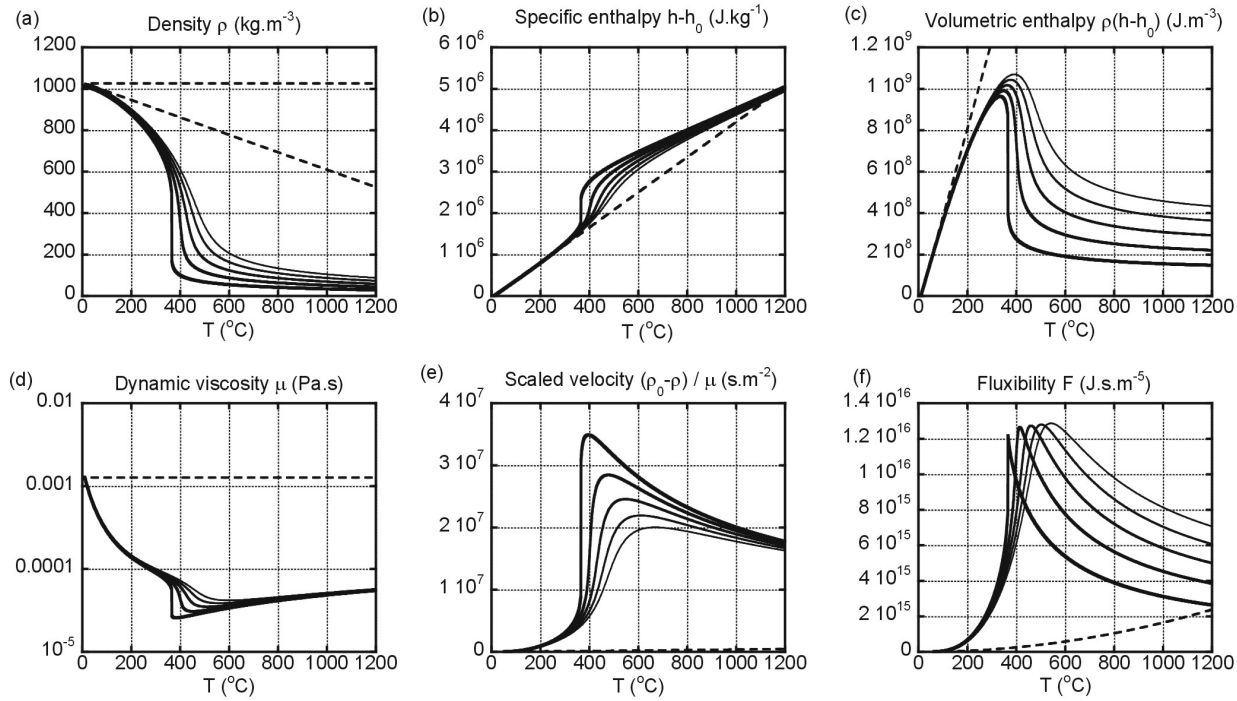

Figure 4. The dependence of the thermodynamic properties of pure water on pressure and temperature. Values are are derived from the steam tables in the HYDROTHERM simulation code [*Hayba and Ingebritsen*, 1994; *Haar et al.*, 1984; *Watson et al.*, 1980; *Sengers and Kamgar–Parsi*, 1984; *Sengers and Watson*, 1986]. Water properties (solid lines) shown at 20 MPa (thickest line), 30 MPa, 40 MPa, 50 MPa and 60 MPa (thinnest line). These pressures correspond to depths of between 2 km and 6 km below sea level. In each case the dashed line shows the values for a 'Boussinesq fluid' for which the temperature dependence is either linearised or ignored. (*a*) The density ρ. (*b*) The specific enthalpy $h-h_0$ (a measure of the energy carried by unit mass of fluid). (*c*) The volumetric enthalpy $\rho(h-h_0)$ (a measure of the energy carried by unit volume of fluid). (*d*) The dynamic viscosity μ. Note logarithmic scale on vertical axis. (*f*) The scaled vertical Darcy velocity $(\rho_0-\rho)/\mu$. The buoyancy–driven Darcy velocity (in $\mathrm{m.s^{-1}}$) is $gk_D(\rho_0-\rho)/\mu$. (*f*) The scaled vertical energy flux or 'fluxibility' $F=\rho(h-h_0)(\rho_0-\rho)/\mu$. The buoyancy–driven energy flux (in $\mathrm{W.m^{-2}}$) is gk_DF.

behaviour is in stark contrast to the behaviour of a Boussinesq fluid, for which the volumetric enthalpy would be:

$$\rho_{Bsq}(h_{Bsq}-h_0)=[c_p\rho_0]\,(T-T_0)\,. \tag{11}$$

We conclude that the Boussinesq approximation for the volumetric enthalpy is valid only for hydrothermal water below about 200°C.

The next thermodynamic variable to appear in the definition of the fluxibility is the dynamic viscosity μ. The viscosity is a measure of the fluid's tendency to resist motion, which for convection is induced by the buoyancy factor $\rho_0-\rho$. Figure 4*d* shows that the viscosity is minimised at ~ 400°C for seafloor hydrothermal pressures. In other words, water 'flows more readily' at ~ 400°C than at any other temperature within the range $0°\mathrm{C}-1200°\mathrm{C}$. When the water is in a liquid–like state the dependence of the dynamic viscosity on temperature can be modelled with an Arrhenius equation: $\mu=\mu_0\exp(\gamma/T-\gamma/T_0)$ where the temperature T is expressed on the absolute (Kelvin) scale, μ_0 and T_0 are constants, and $\gamma\sim 3.3$ K. Thus, for water in the liquid–like state, the viscosity is essentially independent of pressure and decreases as the temperature increases. This is because water molecules are organised into progressively smaller coherent groups as temperature increases, giving a lesser resistance to flow. When water is in the gas–like state, however, the temperature dependence of the viscosity is approximately that of an ideal gas [Batchelor, 1967] and so $\mu\approx\mu_{ref}(T/T_{ref})^{1/2}$ (where T is again expressed in Kelvin and $\mu_{ref}/T_{ref}^{1/2}\sim 1.5\cdot 10^{-6}$ Pa.s.K$^{-1/2}$). For water in the gas–like state the dynamic viscosity is independent of pressure and increases as the temperature increases. This is because the kinetic energy of the gas molecules increases with temperature, so they are better able to transport momentum across the flow. Figure 4*d* shows that the nonlinear temperature dependence of the dynamic viscosity of pure water at hydrothermal conditions is very different to that of a Boussinesq fluid, for which it would be treated as a constant:

$$\mu_{Bsq}=\mu_0. \tag{12}$$

The viscosity of pure water changes by a factor of 10 between 0°C and 200°C and so we conclude that the Boussinesq approximation for dynamic viscosity is inappropriate in hydrothermal systems.

In a cold hydrostatic pressure gradient $g\rho_0$ the vertical Darcy velocity of upwelling fluid is $w=gk_D(\rho_0-\rho)/\mu$. It is therefore helpful to combine the 'density drop' $\rho_0-\rho$ and the viscosity μ to give a 'scaled volume flux' $(\rho_0-\rho)/\mu$. Figure 4*e* shows that the scaled volume flux is maximised at ~ 400°C under hydrothermal conditions. In other words, water at seafloor pressures ascends a cold hydrostatic pressure gradient more quickly at ~ 400°C than at any other

temperature. This effect is caused by the viscosity minimum for water at 400°C (Figure 4*d*). Hotter fluid is always less dense than colder fluid and so has greater tendency to rise (Figure 4*a*). As temperatures rise above ~ 400°C, however, the viscosity μ resisting the flow increases faster than the density drop $(\rho_0 - \rho)$ driving the flow. Above ~ 400°C, therefore, we obtain the counterintuitive result that hotter fluid ascends more slowly than colder fluid, in spite of its greater buoyancy. This nonlinear behaviour is very different to that of a Boussinesq fluid, for which the scaled volume flux depends linearly on temperature:

$$\frac{\rho_0 - \rho_{Bsq}}{\mu_{Bsq}} = \left[\frac{\alpha\rho_0}{\mu_0}\right](T - T_0)\,. \tag{13}$$

Finally, the individual thermodynamic properties discussed above can be combined to give the 'scaled energy flux' or 'fluxibility' F of pure water from equation 8. At ~ 400°C upwelling water ascends most rapidly (Figure 4*e*) and carries a maximum quantity of thermal energy per unit volume (Figure 4*c*). It follows that the fluxibility F of hydrothermal water is maximised between ~ 400°C and ~ 500°C as shown in Figure 4*f*. In contrast, the fluxibility of a Boussinesq fluid is a simple quadratic function of temperature:

$$F_{Bsq} = \left[\frac{\alpha\rho_0^2 c_p}{\mu_0}\right](T - T_0)^2\,. \tag{14}$$

Figure 4*f* shows clearly that the fluxibility maximum for hydrothermal water occurs between 400°C and 500°C. This means that the advective flux gk_DF_U of thermal energy extracted from the reaction zone (measured per unit area at the base of the discharge zone) is maximised within this temperature range. The overall power output of the convection cell, however, depends additionally on the lengthscale L_D of the area through which this flux operates. In order to calculate the total power output of the cell, therefore, we must now consider scaling constraints on the lengthscales L_D and H_R.

5. Scalings in Cartesian geometry

With the fluxibility at the upwelling temperature T_U defined according to equation 8, the energy balance in the reaction zone (equation 7) becomes

$$\frac{L\lambda\,(T_D - T_U)}{L_D H_R} \sim gk_D F_U. \tag{15}$$

The total advective power output Φ_U of the hydrothermal system (measured over a length D of ridge axis) consists of an advective heat flux $\sim gk_DF_U$ flowing through an area $\sim 2L_DD$. It follows that the total advective power output satisfies:

$$\Phi_U \sim 2gk_DF_UDL_D. \tag{16}$$

Scalings for the system can now be calculated as functions of the power output per unit length of ridge axis $[\Phi_U/D]$ and the driving temperature T_D. Equation 16 shows that the product k_DL_D satisfies

$$k_DL_D \sim \frac{[\Phi_U/D]}{2gF_U} \tag{17}$$

while equations 5 and 15 show that the permeability of the reaction zone satisfies

$$k_R \sim \frac{[\Phi_U/D]^3}{8gF_UL\lambda^2\,(T_D - T_U)^2}. \tag{18}$$

Equations 15, 17 and 18 imply that the total power output per unit length of ridge axis satisfies

$$\left[\frac{\Phi_U}{D}\right] \sim 2(gF_U)^{1/3}(\lambda\,(T_D - T_U))^{2/3}L^{1/3}k_R^{1/3}. \tag{19}$$

This shows that the total power output of the system is governed by the permeability of the reaction zone k_R rather than the permeability of the discharge zone k_D.

The thicknesses of the permeable and impermeable conductive layers are given by

$$H_R \sim \frac{\lambda\,(T_D - T_U)\,2L}{[\Phi_U/D]}, \quad H_I \sim \frac{\lambda\,(T_M - T_D)\,2L}{[\Phi_U/D]}. \tag{20}$$

Typical values derived from these scalings are plotted as functions of the power per unit length $[\Phi_U/D]$ and the driving temperature T_D in Figure 5. Models of lithospheric cooling require an average heat flux (conductive plus advective) of order 1 W.m^{-2} to pass through young ($<$ 1 Ma) oceanic crust [Stein and Stein, 1994]. This heat flux corresponds to $[\Phi_U/D] \sim 1$ MW.km^{-1} for a strip of ridge of width 1 km centred on the ridge axis and can probably be considered a minimum. On the other hand $[\Phi_U/D] \sim 1000$ MW.km^{-1} is probably a maximum plausible power output.

We now consider the approximate residence time of fluids in the reaction zone. If the reaction zone has porosity ϕ then fluid moves through the reaction zone at interstitial speed u/ϕ. The approximate magnitude of the residence time of fluid in the reaction zone t_R is therefore given by:

$$t_R \sim \frac{L\phi}{u} = \frac{4\lambda\phi L^2\,(T_D - T_U)\,\rho_U\,(h_U - h_0)}{[\Phi_U/D]^2} \tag{21}$$

from equations 2, 8, 18 and 20. This scaling for the reaction zone residence time is plotted in Figure 5. We note that a power-per-unit-length $[\Phi_U/D] \sim 10$ MW.km^{-1} gives $t_R \sim 10$ years and is consistent with the radioisotope estimates suggesting that t_R lies between 3 and 20 years [Kadko and Moore, 1988; Grasty *et al.*, 1988]. This would imply a reaction zone permeability $k_R \sim 10^{-14}$ m^2 and conductive layers with a thickness of about 100 metres. On the other hand, a power-per-unit-length greater than 100 MW.km^{-1}, which seems plausible, would imply a residence time in the reaction zone of less than a month, a permeability k_R greater than 10^{-12} m^2, and conductive layers no more than a few metres thick.

6. Scalings in axisymmetric geometry

We now consider the approximate scalings for an axisymmetric system above a magma chamber which is circular in plan form. In this case, Figure 1 should be interpreted as having an axis of rotational symmetry about the vertical centre line of the discharge zone. The velocity components (u, w) are then interpreted as being in the radial and vertical directions, but take the same form as before (equations 2 and 3). The conservation of mass, however, is now expressed by the balance:

$$2\pi\rho_U uLH_R \sim \rho_U w\pi L_D^2. \tag{22}$$

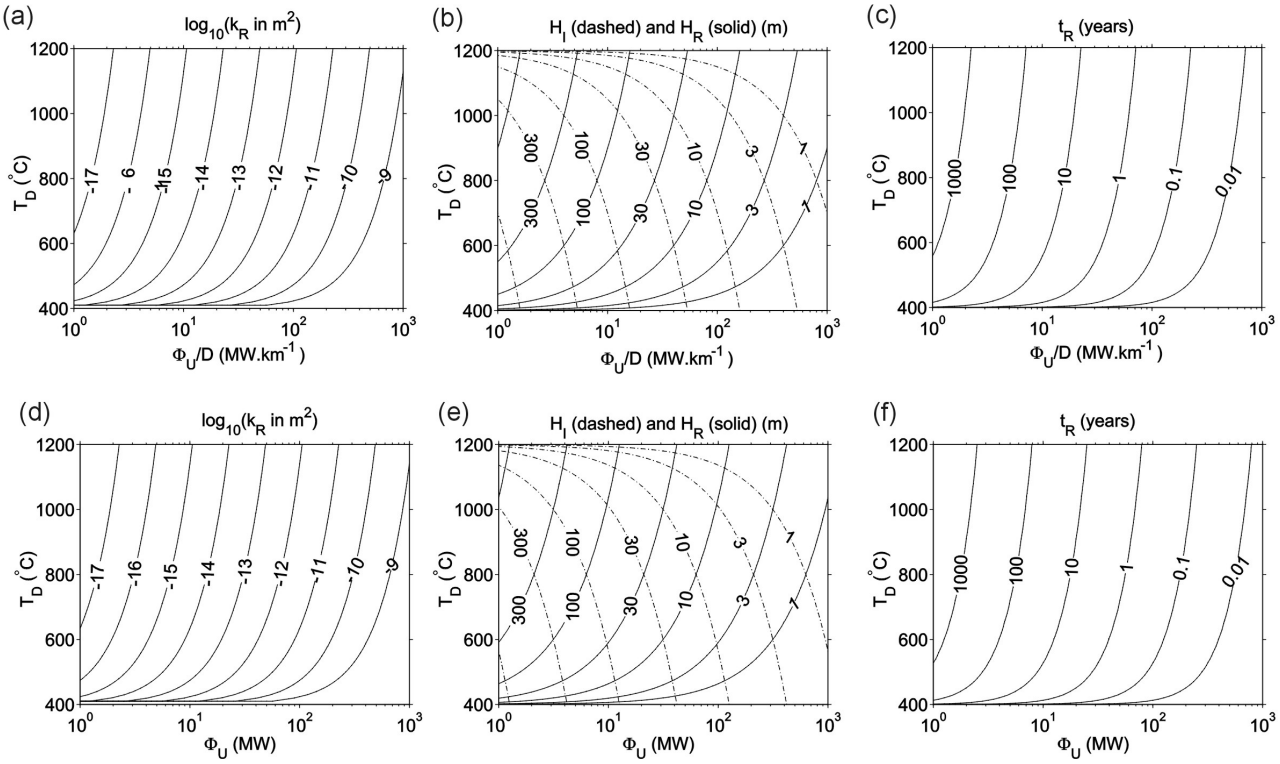

Figure 5. Scalings in 2–d Cartesian and axisymmetric geometry, using typical parameter values: $L = 500$ m, $g = 9.8$ m.s^{-2}, $H = 1000$ m, $\lambda = 2$ W.m^{-1}.K^{-1}, $T_M = 1200°$C, $T_U = 400°$C, $\phi = 0.1$, $F_U = 1.2 \cdot 10^{16}$ J.s.m^{-5} and $\rho_U\,(h_U - h_0) = 10^9$ J.m^{-3}. (a) The permeability k_R of the reaction zone in Cartesian geometry; (b) The thicknesses of the impermeable conductive layer H_I (dashed) and the permeable conductive layer H_R (solid) in Cartesian geometry; (c) The residence time t_R of the reaction zone in Cartesian geometry; (d,e, f) As parts a,b, c but for axisymmetric geometry.

Using equations 2 and 3 it follows that the conservation of mass in the reaction zone is expressed by the balance:

$$2k_R H_R^2 \sim k_D L_D^2. \tag{23}$$

The total advective power output Φ_U of the hydrothermal system consists of an advective heat flux $\sim gk_D F_U$ flowing through an area πL_D^2. It follows that the total advective power output is, approximately:

$$\Phi_U \sim \pi g F_U k_D L_D^2. \tag{24}$$

An argument analogous to the one used in the Cartesian case shows that the conservation of energy in the reaction zone is expressed by the balance:

$$\frac{\lambda\,(T_D - T_U)}{H_R}\pi L^2 \sim \rho_U\,(h_U - h_0)\,w\pi L_D^2. \tag{25}$$

Equations 3 and 8 can then be used to express the energy balance in the alternative form:

$$\frac{L^2\lambda\,(T_D - T_U)}{L_D^2 H_R} \sim gk_D F_U. \tag{26}$$

It is then possible to derive expressions analogous to equations 17, 18 and 20, with the difference that the scalings are now in terms of the total power output Φ_U rather than the power-per-unit-length Φ_U/D. The scalings for the permeabilities are:

$$k_D L_D^2 \sim \frac{\Phi_U}{\pi g F_U}, \tag{27}$$

$$k_R \sim \frac{\Phi_U^3}{2\pi^3 g F_U L^4 \lambda^2\,(T_D - T_U)^2}. \tag{28}$$

The total power output of the hydrothermal system in axisymmetric geometry is

$$\Phi_U \sim 2^{1/3}\pi(gF_U)^{1/3}(\lambda(T_D - T_U))^{2/3}L^{4/3}k_R^{1/3} \tag{29}$$

and so is governed by the permeability in the reaction zone rather than in the discharge zone. The thicknesses of the permeable and impermeable conductive layers are given by

$$H_R \sim \frac{\lambda\,(T_D - T_U)\,\pi L^2}{\Phi_U}, \quad H_I \sim \frac{\lambda\,(T_M - T_D)\,\pi L^2}{\Phi_U} \tag{30}$$

From equations 2, 8, 28 and 30, the residence time t_R of fluid in the reaction zone is given by:

$$t_R \sim \frac{L\phi}{u} = \frac{2\pi^2\lambda\phi L^4\,(T_D - T_U)\,\rho_U\,(h_U - h_0)}{\Phi_U^2}. \tag{31}$$

The scalings for axisymmetric geometry are shown in Figure 5 and give similar results to those for Cartesian geometry. In axisymmetric geometry, a residence time $t_R \sim 10$ years is consistent with a total power output $\Phi_U \sim 10$ MW, a reaction zone permeability $k_R \sim 10^{-14}$ m^2 and conductive layers with thicknesses between 30 and 100 metres.

7. Do hydrothermal systems maximise the overall rate of heat transfer?

In the sections above we constructed a simple model for the structure of a hydrothermal convection cell. The model

cell operates between a driving temperature $T_D \leq 1200°\mathrm{C}$ and a cold temperature $T_0 \approx 0°\mathrm{C}$. The model requires values for the driving temperature T_D and the upwelling temperature T_U to be chosen. Empirical evidence and numerical simulations suggest that $T_U \approx 400°\mathrm{C}$ in real seafloor systems, and so we chose to set $T_U = 400°\mathrm{C}$ in the previous sections. We now consider whether there is any physical basis for this choice by considering the overall rate of heat transfer (i.e. the power output Φ_U) of the hydrothermal cell.

In the model convection cell, the total power output of the hydrothermal system depends on the driving temperature T_D and the upwelling temperature T_U in the same manner in both Cartesian and axisymmetric geometries (equations 19 and 29). In both cases, this dependence takes the form

$$\Phi_U \propto \left[F_U \left(T_D - T_U\right)^2\right]^{1/3}. \tag{32}$$

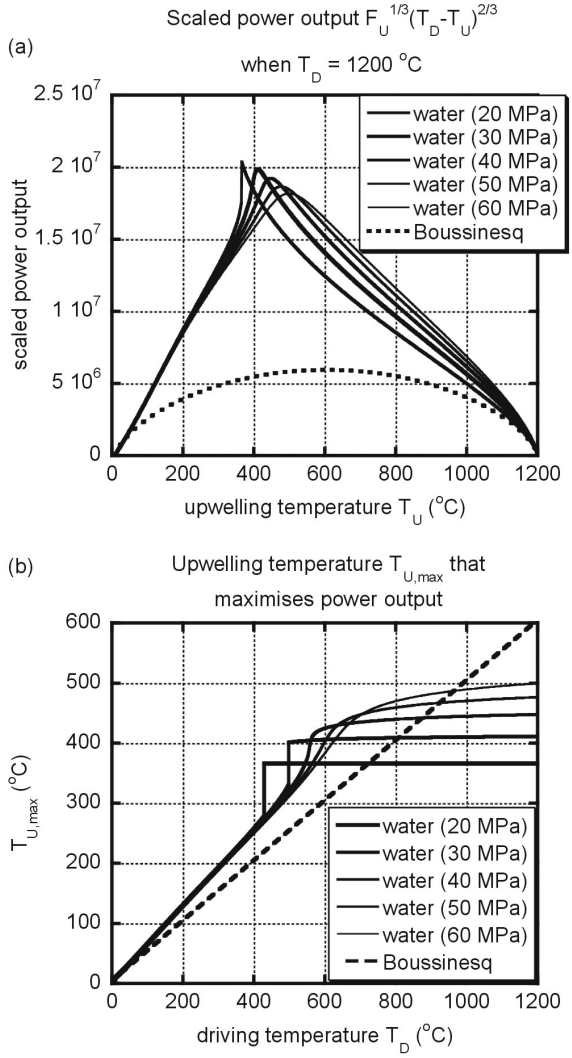

Figure 6. The power output of a porous convection cell containing pure water (solid lines) and a Boussinesq fluid (dashed lines). (a) The total power output Φ_U as a function of upwelling temperature T_U (equation 32) with $T_D = 1200°\mathrm{C}$ and $T_0 = 0°\mathrm{C}$. Similar results are obtained for other values of $T_D \leq 1200°\mathrm{C}$. (b) The temperature $T_{U,max}$ that maximises the total power output Φ_U as a function of driving temperature T_D.

This dependence of total power output on upwelling temperature is shown in Figure 6a – for pure water at hydrothermal pressures as well for a hypothetical Boussinesq fluid – in the case where $T_D = 1200°\mathrm{C}$. When the full thermodynamic properties of water are retained, the total power output is seen to be maximised when the upwelling temperature is about 400°C. It follows that the upwelling temperature that is observed in real systems ($T_U \approx 400°\mathrm{C}$) is approximately equal to the value $T_{U,max}$ that maximises the total power output in our model system. Figure 6b shows, furthermore, that this result holds for any value of the driving temperature T_D up to the maximum possible value 1200°C – the upwelling temperature $T_{U,max}$ that maximises the power output is approximately 400°C for any driving temperature between $\sim 500°\mathrm{C}$ and $\sim 1200°\mathrm{C}$. This behaviour is a consequence of the nonlinear thermodynamic properties of water. (In the case of a Boussinesq fluid, the upwelling temperature that maximises power output is simply the arithmetic mean of the cold temperature and the driving temperature: equations 14 and 32 give $T_{U,max} = (T_0 + T_D)/2$). In the light of these observations, we note that (1) it is possible to 'choose' a value for the upwelling temperature T_U by maximising the power output Φ_U and (2) this choice is essentially independent of the driving temperature T_D. But is there any physical justification for this procedure?

For some years it has been speculated that convective systems achieve a steady state in which the overall heat transport is maximised, subject to the constraints imposed on the system. Originally, this hypothesis was formulated in the context of the spacing of plumes in turbulent convection in a pure fluid [Malkus, 1954; Howard, 1963; Howard, 1964] but the idea has been extended to the case of convection in a porous medium [Busse and Joseph, 1972]. In the context of hydrothermal systems, the so–called 'Malkus hypothesis' has been discussed in relation to the 'preferred' spacing between hydrothermal plumes [Wilcock, 1998]. Here we speculate that it might be reasonable to extend the concept to the emergence of a 'preferred' upwelling temperature. Recently, arguments from statistical mechanics have been used to derive a general 'Principle of Maximum Entropy Production' for arbitrary dissipative systems which, if true, implies that convective systems achieve steady states in which the overall rate of heat transport is maximised subject to any external constraints [Dewar, 2003; Lorenz, 2003]. This is an interesting area of active research, but it is not yet clear whether or not convective systems really do behave in this way. Nonetheless, it is safe to make the following statement: if convective systems do maximise heat transfer in the steady state, and if our model is reasonable, then the upwelling temperature in a real hydrothermal system would have to be $T_U \sim 400°\mathrm{C}$ for any driving temperature $T_D \geq 500°\mathrm{C}$.

8. Conclusions

It has been shown that a simple 2-d model of hydrothermal convection is sufficient to reproduce many of the expected features of a hydrothermal convection cell, providing that the full nonlinear properties of water are retained. The model, which does not rely on inhomogeneous permeability or phase separation, is able to reproduce the thin reaction zone and vent temperatures limited to 400°C which are characteristic of all seafloor hydrothermal systems. This suggests that the dynamics associated with inhomogeneous permeability or phase separation are not required in order to

explain convection cell structure, although both phenomena are undoubtedly important in active hydrothermal systems.

The scaling analysis presented takes account of the nonlinear thermodynamic properties of water where possible. It has been shown how the lengthscales, residence times and total power output of a hydrothermal system depend on its power output.

Notation

c_p	specific heat capacity (cold water) (4.2 kJ.kg^{-1}.K^{-1})
F	'fluxibility' (J.s.m^{-5})
F_U	'fluxibility' of upwelling water ($1.2 \cdot 10^{16}$ J.s.m^{-5})
g	gravitational acceleration (9.8 m.s^{-2})
H	depth of magma chamber (1000 m)
H_I	thickness of impermeable layer (m)
H_R	thickness of reaction zone (m)
h	specific enthalpy of water (J.kg^{-1})
k_D	permeability in discharge zone (m^2)
k_R	permeability in reaction zone (m^2)
L	half–width of magma chamber (500 m)
L_D	half–width of base of discharge zone
p	pressure (Pa)
r	radial coordinate (m)
T_0	seawater temperature (2°C)
T_M	temperature of magma chamber (1200°C)
T_U	temperature of upwelling water (400°C)
T_V	vent temperature (350°C)
t_R	residence time in reaction zone (s)
u	horizontal Darcy velocity (m.s^{-1})
w	vertical Darcy velocity (m.s^{-1})
x	horizontal coordinate (m)
z	vertical coordinate (m)
α	thermal expansivity of cold water ($5 \cdot 10^{-4}$ K^{-1})
β	ideal gas parameter ($2.3 \cdot 10^{-3}$ kg.K.J^{-1})
γ	Arrhenius equation parameter (3.3 K)
λ	thermal conductivity (2 W.m^{-1}.K^{-1})
μ_0	dynamic viscosity of cold water ($1.27 \cdot 10^{-3}$ Pa.s)
ρ_0	density of cold water (1025 kg.m^{-3})
Φ_U	power output (W)
ϕ	porosity (0.1)

Acknowledgments. We thank Bob Lowell and an anonymous referee for helpful comments on an earlier draft. T.E.J. acknowledges support from the Newton Trust, the BP Institute and NERC studentship number GT4/96/54/E. A.S. acknowledges support from NSF grant OCE9901563, through Woods Hole Oceanographic Institution subcontract A100110 with Earth-Ocean Systems Ltd.

References

Alt, J.C., Subseafloor processes in mid–ocean ridge hydrothermal systems, in 'Seafloor hydrothermal systems: Physical, Chemical, Biological and Geological interactions', (ed. Humphris, S.E. et al.), *Geophysical Monograph Series, 91*, 85 – 114, 1995.

Anderko, A. and K.S. Pitzer, Equation–of–state representation of phase equilibria and volumetric properties of the system NaCl–H2O above 573 K, *Geochim. Cosmochim. Acta, 57*,1657 – 1680, 1993.

Batchelor, G.K., An Introduction to Fluid Dynamics, pp. 1 – 70 (Cambridge University Press, Cambridge), 1967.

Berndt, M.E., Seyfried, W.E. and J.W. Beck, Hydrothermal alteration processes at mid–ocean ridges: experimental and theoretical constraints from Ca and Sr exchange reactions and isotopic ratios, *J. Geophys. Res., 93*, 4573 – 4583, 1988.

Berndt, M.E., Seyfried, W.E. and D.R. Janecky, Plagioclase and epidote buffering of cation ratios in mid–ocean ridge hydrothermal fluids: experimental results in and near the supercritical region, *Geochim. Cosmochim. Acta, 53*, 2283 – 2300, 1989.

Bischoff, J.L. and R.J. Rosenbauer, An empirical equation of state for hydrothermal seawater (3.2 percent NaCl), *Amer. J. Sci., 285*, 725 – 763, 1985.

Bischoff, J.L. and K.S. Pitzer, Phase relations and adiabats in boiling seafloor geothermal systems, *Earth Planet. Sci. Lett., 75*, 327 – 338, 1985.

Busse, F.H. and D.D. Joseph, Bounds for heat transport in a porous layer, *J. Fluid Mech., 54*, 521 – 543, 1972.

Campbell, A.C., Palmer, M.R., Klinkhammer, G.P., Bowers, T.S., Edmond, J.M., Lawrence, J.R., Casey, J.F., Thomson, G., Humphris, S., Rona, P. and J.A. Karson, Chemistry of hot springs on the Mid–Atlantic Ridge, *Nature, 335*, 514 – 519, 1988.

Cann, J.R. and M.R. Strens, Black smokers fuelled by freezing magma, *Nature, 298*, 147 – 149, 1982.

Cherkaoui, A.S.M. and W.S.D. Wilcock, Laboratory studies of high Rayleigh number circulation in an open–top Hele–Shaw cell: An analog to mid–ocean ridge hydrothermal systems, *J. Geophys. Res., 106*, 10983 – 11000, 1998.

Cherkaoui, A.S.M. and W.S.D. Wilcock, Characteristics of high Rayleigh number two–dimensional convection in an open–top porous layer heated from below, *J. Fluid Mech., 394*, 241 – 260, 1999.

Cowan, J. and J. Cann, Supercritical two–phase separation of hydrothermal fluids in the Troodos ophiolite, *Nature, 333*, 259 – 261, 1988.

Detrick, R.S., Buhl, P., Vera, E., Mutter, J., Orcutt, J., Madsen, J. and T. Brocher, Multi–channel seismic imaging of a crustal magma chamber along the East Pacific Rise, *Nature, 326*, 35 – 41, 1987.

Dewar, R., Information Theory explanation of the fluctuation theorem, maximum entropy production and self–organized criticality in non–equilibirum stationary states, *J. Phys. A, 36*, 631 – 641, 2003.

Dickson, P., Schultz, A., and A. Woods, Preliminary modelling of hydrothermal circulation within mid–ocean ridge sulphide structures, in 'Hydrothermal Vents and Processes', (ed. Parson, L.M. et al.), *Geological Society Special Publication, 87*, 145 – 157, 1995.

Dickson, P.C., Modelling fluid flow in seafloor hydrothermal systems, Ph.D. thesis, University of Cambridge, 218 pp., 1997.

Doering, C.R. and P. Constantin, Bound for heat transport in a porous layer, *J. Fluid Mech., 376*, 263 – 296, 1998.

Dunn, J.C. and H.C. Hardee, Superconvecting geothermal zones, *J. Volc. Geo. Res., 11*, 189 – 201, 1981.

Dunn, R.A., Toomey, D.R. and S.C. Solomon, Three–dimensional structure and physical properties of the crust and shallow mantle beneath the East Pacific Rise at 9°30′N, *J. Geophys. Res., 105*(B10), 23537 – 23555, 2000.

Elder, J.E., Geothermal Systems, pp. 180 – 187 (Academic Press, London), 1981.

Faust, C.R. and J.W. Mercer, Geothermal Reservoir Simulation 1. Mathematical Models for Liquid– and Vapor–Dominated Hydrothermal Systems, *Water Res. Res., 15*, 23 – 30, 1979.

Fournier, R.O., The transition from hydrostatic to greater than hydrostatic fluid pressure in presently active continental hydrothermal systems in crystalline rock, *Geophys. Res. Lett., 18*, 955 – 958, 1991.

Germanovich, L.N. and R.P. Lowell, Percolation theory, thermoelasticity, and discrete hydrothermal venting in the Earth's crust, *Science, 255*, 1564 – 1567, 1992.

Gillis, K.M. and M.D. Roberts, Cracking at the magma–hydrothermal transition: evidence from the Troodos Ophiolite, Cyprus, *Earth Plan. Sci. Lett., 169*, 227 – 244, 1999.

Graham, M.D. and P.H. Steen, Plume formation and resonant bifurcations in porous–media convection, *J. Fluid Mech., 272*, 67 – 89, 1994.

Grasty, R.L., Smith, C.W., Franklin, J.M. and I.R. Jonasson, Radioactive orphans in barite–rich chimneys, Axial Caldera, Juan de Fuca Ridge, *Can. Min., 26*, 627 – 636, 1988.

Haar, L., Gallagher, J.S. and G.S. Kell, NBS/NRC Steam Tables, 320pp. (Hemisphere, New York), 1984.

Hayba, D.O. and S.E. Ingebritsen, The computer model HYDROTHERM, a three–dimensional finite–difference model to simulate ground–water flow and heat transport in the temperature range of 0 to 1,200 degrees Celsius, *U.S. Geological Survey Water–Resources Investigations Report, 94–4045*, 1994.

Howard, L.N., Heat transport by turbulent convection, *J. Fluid Mech., 17*, 405 – 432, 1963.

Howard, L.N., Convection at high Rayleigh number, *Proc. 11th Intl. Cong. Appl. Mech., Munich*, 1109 – 1115, 1964.

Ingebritsen, S.E. and D.O. Hayba, Fluid flow and heat transport near the critical point of H2O, *Geophys. Res. Lett., 21*, 2199 – 2202, 1994.

Johnson, J.W. and D. Norton, Critical phenomena in hydrothermal systems: state, thermodynamic, electrostatic, and transport properties of H2O in the critical region, *Amer. J. Sci., 291*, 541 – 648, 1991.

Jupp, T. and A. Schultz, A thermodynamic explanation for black smoker temperatures, *Nature, 403*, 880 – 883, 2000.

Kadko, D. and W. Moore, Radiochemical constraints on the crustal residence time of submarine hydrothermal fluids: Endeavour Ridge, *Geochim. Cosmochim. Acta, 52*, 659 – 668, 1988.

Lapwood, E.R., Convection of a fluid in a porous medium, *Proc. Cam. Phil. Soc., 44*, 508 – 521, 1948.

Lister, C.R.B., On the penetration of water into hot rock, *Geophys. J. Roy. Ast. Soc., 39*, 465 – 509, 1974.

Lister, C.R.B., Heat transfer between magmas and hydrothermal systems, or, six lemmas in search of a theorem, *Geophys. J. Int., 120*, 45 – 59, 1995.

Lorenz, R.D., Full Steam Ahead – Probably, *Science, 299*, 837 – 838, 2003.

Lowell, R.P., Van Cappellen, P. and L. Germanovich, Silica precipitation in fractures and the evolution of permeability in hydrothermal upflow zones, *Science, 260*, 192 – 194, 1993.

Lowell, R.P. and L.N. Germanovich, On the temporal evolution of high–temperature hydrothermal systems at ocean ridge crests, *J. Geophys. Res., 99*, 565 – 575, 1994.

Lowell, R.P., Rona, P.A. and R.P. Von Herzen, Seafloor hydrothermal systems, *J. Geophys. Res., 100*, 327 – 352, 1995.

Lowell, R.P., and P.A. Rona, Seafloor hydrothermal systems driven by serpentinization of peridotite, *Geophys. Res. Lett., 29*(11), Art. No. 1531, 2002.

Lowell, R.P., Yao, Y. and L.N. Germanovich, Anhydrite precipitation and the relationship between focused and diffuse flow in seafloor hydrothermal systems, *J. Geophys. Res., 108*(B9), 2424, doi:10.1029/2002JB002371, 2003.

Lowell, R.P. and L.N. Germanovich, Hydrothermal processes at mid–ocean ridges: results from scale analysis and single–pass models, *AGU Monograph* **give details when known**, 2004.

Malkus, W.V.R., The heat transport and spectrum of thermal turbulence, *Proc Roy. Soc. A, 225*, 196 – 212, 1954.

Morton, J.L. and N.H. Sleep, A Mid–Ocean Ridge Thermal Model: Constraints on the Volume of Axial Hydrothermal Heat Flux, *J. Geophys. Res., 90*(B13), 11345 – 11353, 1985.

Norton, D. and J. Knight, Transport phenomena in hydrothermal systems: cooling plutons, *Amer. J. Sci., 277*, 937 – 981, 1977.

Pascoe, A.R. and J.R. Cann, Modelling diffuse hydrothermal flow in black smoker vent fields, in 'Hydrothermal Vents and Processes', (ed. Parson, L.M. et al.), *Geol. Soc. Spec. Pub., 87*, 159 – 173, 1995.

Phillips, O.M., Flow and reactions in permeable rocks, pp. 245–264 (Cambridge University Press, Cambridge), 1991.

Richardson, C.J., Cann, J.R., Richards, H.G. and J.G. Cowan, Metal–depleted toot zones of the Troodos ore–forming system, *Earth Plan. Sci. Lett., 84*, 243 – 253, 1987.

Schultz, A., Delaney, J.R. and R.E. McDuff, On the partitioning of heat flux between diffuse and point source seafloor venting, *J. Geophys. Res., 97*(B9), 12,299 – 12,314, 1992.

Seewald, J.S. and W.E. Seyfried, The effect of temperature on metal mobility in subseafloor hydrothermal systems: constraints from basalt alteration experiments, *Earth Plan. Sci. Lett.,101*, 388 – 403, 1990.

Sengers, J.V. and B. Kamgar–Parsi, Representative equations for the viscosity of water substance, *J. Phys. Chem. Ref. Data, 13*, 185 – 205, 1984.

Sengers, J.V. and J.T.R. Watson, Improved international formulation for the viscosity and thermal conductivity of water substance, *J. Phys. Chem. Ref. Data, 15*, 1291 – 1314, 1986.

Seyfried, W.E. and J.L. Bischoff, Low temperature basalt alteration by seawater: an experimental study at 70°C and 150°C, *Geochim. Cosmochim. Acta, 43*, 1937 – 1947, 1979.

Seyfried, W.E. and M.J. Mottl, Hydrothermal alteration of basalt by seawater under seawater–dominated conditions, *Geochim. Cosmochim. Acta, 46*, 985 – 1002, 1982.

Stein, C.A. and S. Stein, Constraints on hydrothermal heat flux through the oceanic lithosphere from global heat flow, *J. Geophys. Res., 99*(B2), 3081 – 3095, 1994.

Straus, J.M. and G. Schubert, Thermal convection of water in a porous medium: effects of temperature– and pressure–dependent thermodynamic and transport properties, *J. Geophys. Res., 82*, 325 – 333, 1977.

Toomey, D.R., Solomon, S.C. and G.M. Purdy, Tomographic imaging of the shallow crustal structure at the East Pacific Rise at 9°30′N, *J. Geophys. Res., 99*(B12), 24135 – 24157, 1994.

Van Wylen, G.J. and R.E. Sonntag, Fundamentals of classical thermodynamics, SI version, 2nd edition, 744 pp., (John Wiley and Sons, New York), 1978.

Von Damm, K.L., Edmond, J.M., Grant, B., Measures, C.I., Walden, B. and R.F. Weiss, Chemistry of submarine hydrothermal solutions at 21°N, East Pacific Rise, *Geochim. Cosmochim. Acta, 49*, 2197 – 2220, 1985.

Von Damm, K.L. and J.L. Bischoff, Chemistry of Hydrothermal Solutions from the Southern Juan de Fuca Ridge, *J. Geophys. Res., 92*(B11), 11334 – 11346, 1987.

Von Damm, K.L. Lilley, M.D., Shanks, W.C., Brockington, M., Bray, A.M., O'Grady, K.M., Olson, E., Graham, A., Proskurowski, G. and the SouEPR Science Party, Extraordinary phase separation and segregation in vent fluids from the southern East Pacific Rise, *Earth Planet. Sci. Lett., 206*, 365 – 378, 2003.

Watson, J.T.R., Basu, R.S. and J.V. Sengers, An improved representative equation for the dynamic viscosity of water substance, *J. Phys. Chem. Ref. Data, 9*, 1255 – 1290, 1980.

Wilcock, W.S.D., Cellular convection models of mid–ocean ridge hydrothermal circulation and the temperatures of black smoker fluids, *J. Geophys. Res., 103*, 2585 – 2596, 1998.

Wilson, E.N., Hardie, L.A. and O.M. Phillips, Dolomitization front geometry, fluid flow patterns and the origin of massive dolomite: the triassic Lateman buildup, Northern Italy, *Amer. J. Sci., 290*, 741 – 796, 1990.

T. E. Jupp, Centre for Ecology and Hydrology, Monks Wood, Abbots Ripton, Huntingdon, Cambridgeshire PE28 2LS, U.K. (tju@ceh.ac.uk)

A. Schultz, College of Oceanic and Atmospheric Sciences, Oregon Sate University, 104 COAS Admin. Bldg., Corvallis, OR 97331-5503, USA. (adam@coas.oregonstate.edu)

(Received _____.)